Arab J Sci Eng
DOI 10.1007/s13369-017-2934-z

RESEARCH ARTICLE - CHEMICAL ENGINEERING

Removal of Copper and Lead using Banana Biochar in Batch Adsorption Systems: Isotherms and Kinetic Studies

M. T. Amin[1,2] · **A. A. Alazba**[1,3] · **M. Shafiq**[1]

Received: 19 July 2017 / Accepted: 26 October 2017

Abstract This study involved investigating the adsorption potential of biochar prepared from banana peel for the removal of copper (Cu^{2+}) and lead (Pb^{2+}). Process parameters for batch adsorption including contact time, pH, adsorbent dose, and initial metal concentrations were optimized. The time at which the equilibrium adsorption was attained was recoded as 30 min with a higher removal efficiency of Pb^{2+} when compared to Cu^{2+}. Optimum removal was observed at a pH of approximately 5.5 and 9 for Cu^{2+} and Pb^{2+}, respectively. A linear increase in metal removal efficiency was achieved with increases in the adsorbent dose from 0.2 to 1.4 g. The latter was estimated as the optimum adsorbent dose. A 50–70% decrease in removal efficiency was observed when the initial Cu^{2+} and Pb^{2+} concentrations were increased from 50 to 300 mg L^{-1} and from 200 to 1000 mg L^{-1}, respectively. Among the isotherm models, the Freundlich model agreed best with the experimental data for Pb^{2+} while the Langmuir model exhibited a better ability to describe the adsorption of Cu^{2+} with each model providing the highest respective coefficient of determination. A pseudo-second-order kinetic model better described the kinetic behavior of both metal ions on the investigated adsorbent, namely banana biochar.

Keywords Adsorption · Banana Biochar · Cu^{2+} · Freundlich · Langmuir · Process parameters · Pb^{2+} · Pseudo-second-order

1 Introduction

A huge quantity of untreated wastewater from industry, agriculture, and households is discharged into natural water bodies including oceans, rivers, and lakes every day [1]. Consequently, these water bodies are becoming increasingly polluted. The untreated wastewater contains a high amount of hazardous organic and inorganic contaminants [2]. Among these, metallic contaminants are considered the most hazardous owing to their long-term persistency and non-biodegradability [3]. These metals can cause severe adverse effects in humans, animals, and plants, and harm aquatic life [4]. Acute or chronic exposure of humans to these metals causes a range of health problems including cancer, blood pressure, paralysis, blood sugar, tumors, liver and lung failures, joint disease, brain hemorrhage, and sudden death [5–8]. Over the past few decades, the elimination of these rapidly increasing heavy metals from wastewaters constitutes a major challenge in research to ensure that these wastewaters are fit for reuse or discharge to the environment [9,10].

Adsorption is a widely used physical separation method for the removal of hazardous heavy metals from wastewater, with commonly modified adsorbents including activated carbon, alumina, oxides, resins, and silica [11,12]. While these adsorbents possess high reactivity and metal ion selectivity, their expensive preparation methods also generate toxic wastes. This has resulted in a continuing search for inexpensive, abundant, and readily available adsorbents. Specifically, a few recent studies investigated the use of waste materials

✉ M. T. Amin
mtamin@ksu.edu.sa

[1] Alamoudi Water Research Chair, King Saud University, P. O. Box 2460, Riyadh 11451, Kingdom of Saudi Arabia

[2] Department of Environmental Sciences, COMSATS Institute of Information Technology, Abbottabad 22060, Pakistan

[3] Agricultural Engineering Department, King Saud University, P. O. Box 2460, Riyadh 11451, Kingdom of Saudi Arabia

Published online: 13 November 2017

and by-products as adsorbents for heavy metal removal such as orange peel, date palm tree waste, rice husks, wheat straws, and tobacco stems [13–17]. Current research that focuses on adsorbents derived from the aforementioned or similar materials concluded that the conversion of waste materials into biochar corresponds to the best solution to provide adsorbents for waste management and environmental protection.

Biochar is a potential adsorbent material that is a carbon-rich form of charcoal produced by pyrolysis (heating) under limited oxygen conditions from the waste biomass of fruit peels, cattle manure, peat, and wood at temperatures between 350 and 800 °C [18]. Biochar is an ideal adsorbent for removing contaminants from wastewater owing to specific properties including its porous structure, high specific surface area, cation exchange capacity, and abundant surface functional groups [19]. Several studies have reported that biochar possesses an excellent ability to remove contaminants including heavy metals and organic pollutants from aqueous solutions [20–26]. The production of biochar is cheaper when compared to activated carbon because it has lower energy requirements. Furthermore, biochar feedstocks are mainly acquired from agricultural biomass, and this is one of the most abundant renewable resources. Several feedstocks including crop residues, wood biomass, animal litters, and solid wastes were utilized to produce biochar [27].

In the study, Cu^{2+} and Pb^{2+} adsorption was investigated using biochar from banana peel in a batch experiment. The banana peel biochar was prepared at a temperature of 600 °C in a muffle furnace. The Cu^{2+} and Pb^{2+} removal efficiency/adsorption capacity with the use of biochar was obtained through batch experiments. Different isotherm models were applied to the experimental data, and adsorption kinetics were investigated using pseudo-first-order and pseudo-second-order reaction kinetics.

2 Materials and Methods

2.1 Chemicals and Reagents

Stock solutions of Cu^{2+} (1000 mg L^{-1}) and Pb^{2+}(1000 mg L^{-1}) were prepared by dissolving appropriate amounts of copper sulfate pentahydrate ($CuSO_4 \cdot 5H_2O$; AR grade Merck, Germany) and lead nitrate (Pb $(NO_3)_2$), Tianjin Benchmark Chemical Reagent Co., Ltd. Tianjin, China) in ultra-pure water (Milli-Q integral water dispenser) in 1000-mL volumetric flasks. The stock solutions were stored at 4 °C for long-term use and preserved by the addition of 2 mL of concentrated HCl. To generate different initial concentrations of metal ions, serial dilutions of the 1000 mg L^{-1} stock solutions were prepared in distilled-deionized water. Solutions of 0.1 M HCl and 0.1 M NaOH were used to prepare initial solutions with a range of pH values as measured with a microprocessor-based pH meter (PHS-3CW, China).

2.2 Adsorbent Preparation

Banana peel was collected from different places in Riyadh, Saudi Arabia and was washed several times prior to drying in the sun for approximately a week with an average daily temperature of approximately 35–40 °C. At the end of the week, the banana peel was placed in an oven for 3 h at 70 °C. The dried mass of banana peel was crushed in a normal coffee grinder to obtain an average particle size in the range of 0.75–1 mm. The dried and ground powder was packed in a lid-covered crucible and pyrolyzed for 3 h at 600 °C in a box furnace (Nabertherm, B-150, Germany) with a heating rate of 5 °C per minute. The prepared biochar was sieved to obtain an average particle size $\leq$ 100 μm and stored in an air-tight container prior for use.

There are a number of studies suggesting that the optimum temperature to produce biochar from plants and fruit waste-based materials is above 500 °C. It has been found that researchers used the temperature ranges from 300 to 600 °C for biochar production [28,29]. But a number of studies concluded that slow pyrolysis up to 350 °C is best for biochar production for fuel purposes, while temperature from 500 or above was the optimum to produce biochar with stable carbon content, high surface area, porosity, and high electrical conductivity [30,31]. Therefore, based on the previous literature, a pyrolysis temperature of 600 °C was selected for the production of biochar using banana peel waste.

2.3 Batch Adsorption Experiments

The batch experiments were performed in a set of 100-mL conical flasks that were placed in a temperature-controlled Wise Cube orbital shaker (Daihan Scientific Co. Ltd, Wisd. ThermoStable IS-20, South Korea). The samples were shaken for a specified time at 220 rpm and 30 °C and were withdrawn from the shaker and were centrifuged at 1000 rpm for 5 min in a centrifuge (Elektromag M815P model) to separate the adsorbate from the solution. Samples were then filtered through nitrocellulose filter paper (0.45 μm) by using a vacuum filtration assembly prior to the measurement of the residual metal concentration in each sample by flame atomic absorption spectrometry (FAAS, Thermo Scientific, ICE 3000 Series, Cambridge, UK).

For statistical analysis including the assessment of experimental errors, all experiments were performed in triplicate and process parameters including the equilibrium time, pH, initial metal concentration, and the adsorbent dose were optimized. The experimental details are listed in the relevant sections.

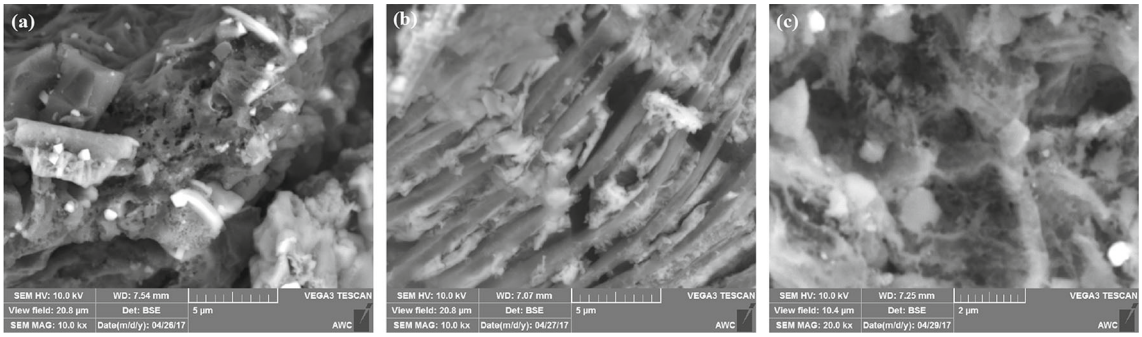

Fig. 1 Scanning electron microscopy images of biochar before (**a**) and after Cu^{2+} (**b**), and Pb^{2+} (**c**) adsorption

The transient adsorption capacity, q_t (mg g^{-1}), is calculated by using the amount of adsorption at time t while the equilibrium adsorption capacity, q_e (mg g^{-1}), and the removal efficiency (sorption percentage) of heavy metal ions from the water phase are calculated by using Eqs. (1) and (2), respectively [32], as follows:

$$q_e = (C_0 - C_e)\, V/M \tag{1}$$

$$\text{Removal}\,(\%) = \frac{(C_0 - C_e)}{C_0} * 100 \tag{2}$$

where C_0 and C_e denote the initial and equilibrium liquid-phase concentrations (mg L^{-1}) of the heavy metal ions, respectively, V denotes the volume of the solution (L), and M denotes the mass of dry adsorbent (g).

3 Results and Discussion

3.1 Characterization of the Biochar Before and After Adsorption

Characterization of the biochar before and after adsorption of heavy metal ions was performed using scanning electron microscopy (SEM, TESCAN VEGA 3 SBU USA) analysis at various magnifications ranging from 500× to 12,000×. The images provide an insight into the appearance of the surfaces of the biochar before and after the adsorption of heavy metal ions (Fig. 1).

Rough asymmetric pores are observed on the surface of the biochar before adsorption, and they enhance the interactions between the biochar and the heavy metal ions. Following the adsorption of Cu^{2+} and Pb^{2+}, the biochar surface becomes smooth and shiny as shown in Fig. 1b and c with closed pore structures. A possible reason for this behavior is attributed to the physicochemical interactions between the functional groups that are present on the surface of the biochar and the heavy metal ions. The crystal structure of the biochar was characterized by powder X-ray diffraction (XRD) using a Rigaku Miniflex diffractometer with Cu Kα radiation (1.5406 Å) operated at 40 kV and 40 mA. Each diffraction scan was run from 5° to 90° 2-theta with steps of 0.02°.

The XRD profile of banana peels (Fig. 2a) at 600 °C indicated a few peaks that were not excessively sharp although these indicate changes in the structure of the charcoal. In this study, more than 70% of the product corresponds to amorphous carbon. This suggests that the pyrolysis reaction is not complete and that amorphous carbon still exists. It is confirmed from the peaks that banana peels are thermally decomposed into fullerene (11.9° and 31.5°) and chaolite (24.05°, 28.6°, 30.1°, 31.5°, 34 39°, and 40.5°). The XRD pattern implied that the pyrolysis products are not pure and contain certain impurities including Fe_2O_3, Fe_3C, and K_2O (Mopoung 2011). After the adsorption of Cu^{2+} and Pb^{2+}, a few new compounds are formed such as cuprite, tolbachite, paramelaconite, and lead azide. However, the peaks of these compounds are not clear in the XRD pattern.

In order to characterize the active surface functional groups of the biochar that may participate in the adsorption of heavy metal ions from aqueous solutions, Fourier transform infrared (FTIR) spectra were recorded between 4000 cm^{-1} and 600 cm^{-1} by using a ZnSe attenuated total reflection (ATR) crystal with a Bruker Alpha-E spectrometer.

Figure 2b shows the various functional groups present on the surface of the biochar before and after adsorption of Cu^{2+} and Pb^{2+}. The banana peel consists of carbohydrates, fiber, proteins, lipids, N–H, O–H, and Si–O functional groups, aliphatic groups, and aromatic rings that are all responsible for adsorption [33]. As shown in Fig. 2b, the peaks in the spectra between 600 and 700 cm^{-1} mainly arise from out-of-plane vibrations of the C–H bond in aromatic and heteroaromatic compounds [34]. Peaks at 831 and 983 cm^{-1} could be the result of the concentration of alkaline earth elements with the peak at 831 cm^{-1} assigned to the C–H out-of-plane bending of an aromatic ring [29]. The peak at 1244 cm^{-1} suggests the presence of a hydrogen-bonded hydroxyl compound [31]. The peak at 1390 cm^{-1} could be assigned to CO_2 [35]. The presence of a carbonyl group at 1605 cm^{-1}

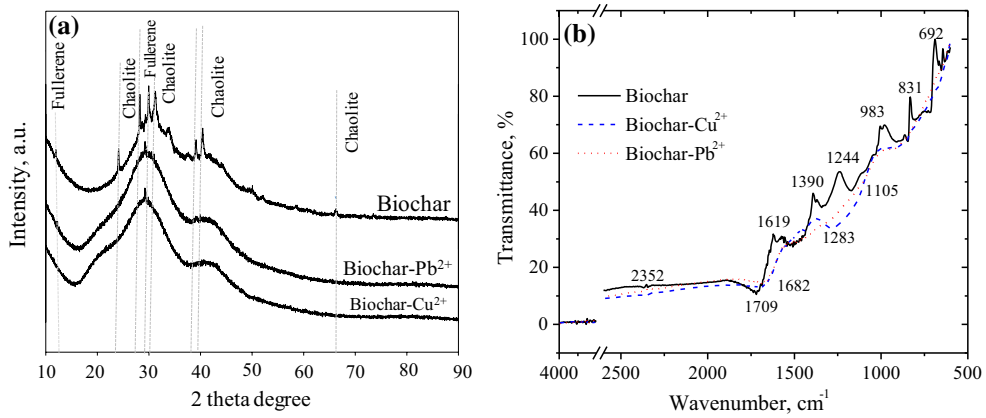

Fig. 2 Comparison of the powder X-ray diffraction results (**a**), and Fourier transform infrared spectroscopy analysis (**b**), before and after adsorption

was also reported for a heated cellulose carbon, and the peak at 1619 cm^{-1} may correspond to –COO– groups and can be assigned to –C=C–C stretches of aromatic ring groups. This indicates the increased stability of banana biochar when compared to banana peel that is due to thermochemical biomass conversion [29,31].

Finally, Brunauer–Emmett–Teller (BET) analyses were performed to determine the surface area of the banana peel and the prepared biochar. The surface area of the biochar was 52.8 $m^2\ g^{-1}$ when compared to 35.24 $m^2\ g^{-1}$ for the banana peel. Thus, an increase of approximately 35% was achieved by heating the dried banana peel at 600 °C during the biochar preparation.

3.2 Effects of Different Process Parameters on Batch Adsorption

Batch adsorption experiments were performed in triplicate by adding different masses (g) of the banana biochar to conical flasks that contained 100 mL of each metal solution. The mass of the adsorbent was adjusted to achieve the desired dose of the biochar (g). Additionally, the effects of the contact time, pH, initial metal concentration and adsorbent dose on the adsorption efficiency were investigated.

3.2.1 Effect of Contact Time

To determine the time taken to reach the adsorption equilibrium, kinetic experiments were performed at a pH value of 5.5 by using initial Cu^{2+} and Pb^{2+} concentrations of 150 and 400 mg L^{-1}, respectively, with corresponding adsorbent doses of 1.0 and 0.5 g. Samples were collected at 1, 3, 5, 10, 15, 30, and 60 min during the first hour with three additional samples collected at 2, 3, and 6 h. The effect of contact time on the adsorption capacity and removal efficiency is shown in Fig. 3.

It is important to determine the residence time to define the efficiency of an adsorbent that is governed by several independent processes [36,37]. Rapid adsorption occurs initially, and a significantly high removal efficiency is observed for both Cu^{2+} and Pb^{2+} during the first 15 min owing to the availability of the uncovered surface area of the adsorbent [38]. This is followed by a slower metal uptake for approximately an additional half an hour. The equilibrium adsorption capacity is reached at approximately 30 min, and insignificant changes in metal adsorption capacities are observed after approximately 1 h, as shown in Fig. 3. The percentage removal of both metals is identical over time although the initial Pb^{2+} concentration was almost double that of Cu^{2+}. Furthermore, the adsorbent dose for Pb^{2+} was twice lower than that for Cu^{2+}.

3.2.2 Effect of Solution pH

The solution pH is one of the factors that significantly affects the adsorption process [39] and pH variations affect the surface charge of the adsorbent and the degree of ionization of the adsorbing heavy metal ions [40,41]. The effect of pH on the adsorption capacity of the studied biochar in terms of percentage removal of Cu^{2+} and Pb^{2+} from the aqueous solution is illustrated in Fig. 4. Batch experiments were conducted in triplicate by using initial metal concentrations of 150 and 400 mg L^{-1}, adsorbent doses of 1.0 and 0.5 g, and contact times of 30 and 15 min for Cu^{2+} and Pb^{2+}, respectively, in the pH range of 3–5.5 for Cu^{2+} and 3–9 for Pb^{2+}.

The adsorption capacity of biochar and the removal efficiency of Cu^{2+} increased when the initial solution pH increased from 3 to 5.5 or from 6 to 9 for Pb^{2+}. A nearly constant adsorption capacity was achieved for Pb^{2+} in the acidic pH range from 3 to 5.5 while the removal efficiency decreased with a further increase in pH above 9 (Fig. 4b). Lower metal uptake at acidic pH values could be due to the presence of

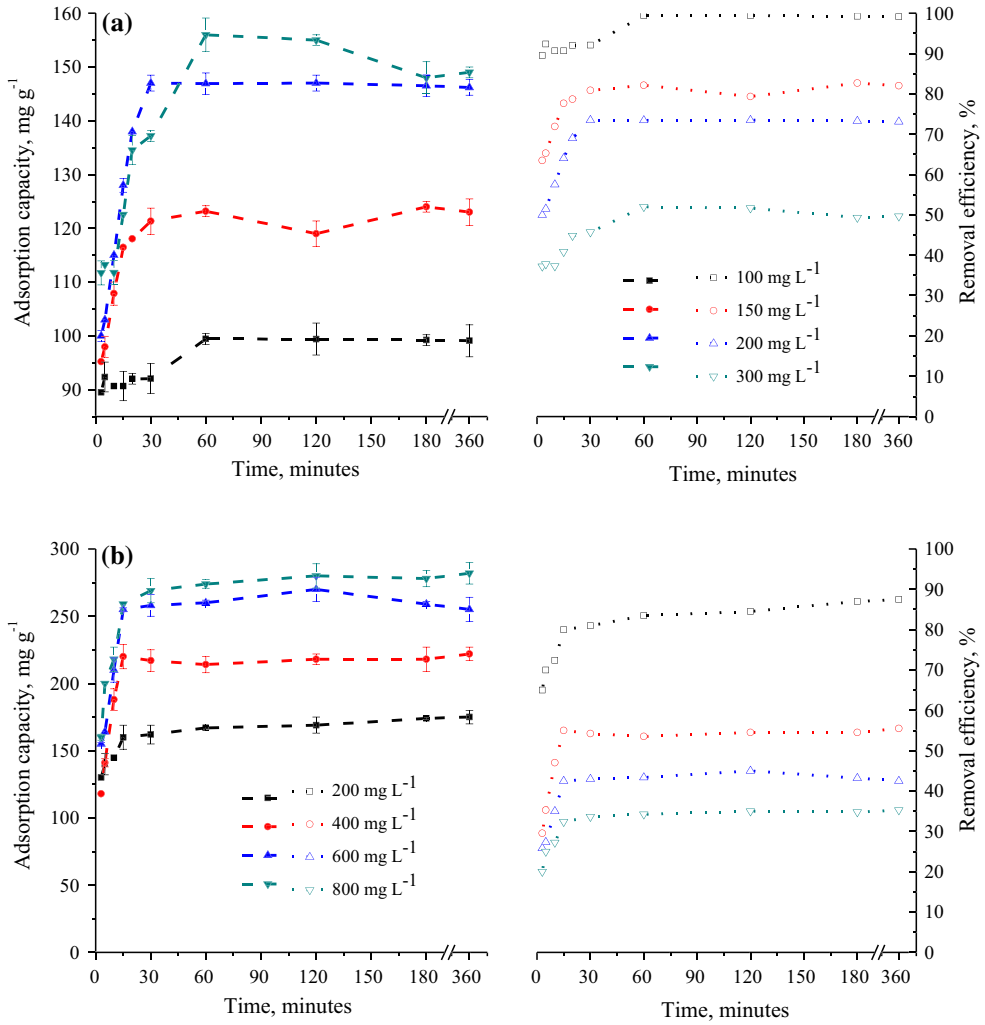

Fig. 3 Effects of contact time on adsorption capacity and removal efficiency of Cu^{2+} (**a**) and Pb^{2+} (**b**) (initial pH 5.5, adsorbent dose 1.0 and 0.5 g for 150 and 400 mg L^{-1} of Cu^{2+} and Pb^{2+}, respectively)

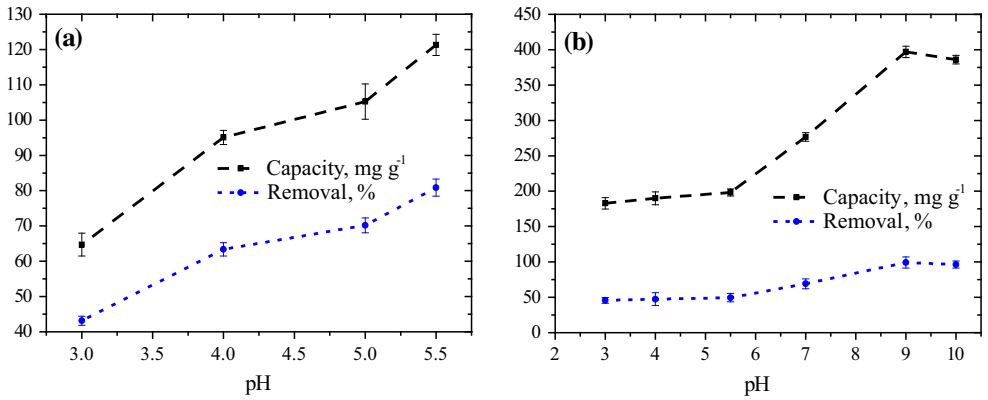

Fig. 4 Effects of solution pH on the adsorption capacity and removal efficiency of Cu^{2+} (**a**) and Pb^{2+} (**b**) (contact time 30 and 15 min, adsorbent dose 1.0 and 0.5 g for 150 and 400 mg L^{-1} of Cu^{2+} and Pb^{2+}, respectively)

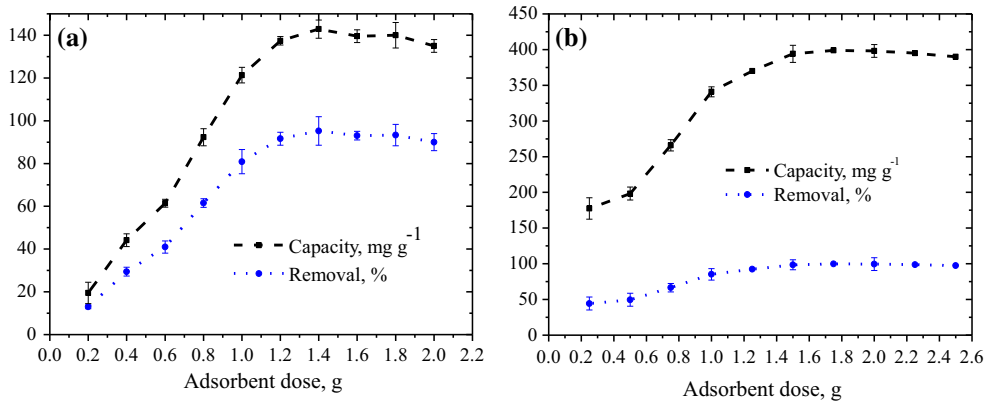

Fig. 5 Effects of adsorbent dose on metal adsorption capacity and removal efficiency of Cu^{2+} (**a**) and Pb^{2+} (**b**) (initial pH 5.5, contact time 30 and 15 min for 150 and 400 mg L^{-1} of Cu^{2+} and Pb^{2+}, respectively)

excess H^+ ions that competes with the divalent metal ions for adsorption sites on the surface of the biochar [42]. Furthermore, lowered electrostatic repulsive interaction between the positively charged metal ions and the surface of the biochar adsorbent due to the decreased positive surface charge density at higher solution pH values results in higher adsorption rates [43]. Additionally, the reduction in negative charges on the surface of the biochar at low pH values resulted in decreased attraction for the positively charged metal cations in the study. The investigated pH dependence shows that electrostatic interactions, ion exchanges, and hydrogen bonding are involved in the adsorption of metal ions by the banana biochar [44,45].

3.2.3 Effect of the Adsorbent Dose

The effect of varying adsorbent (banana biochar) dose on the adsorption capacity and percent removal of the studied heavy metal ions is depicted in Fig. 5 in the range of 0.2–1.6 g and 0.2–2.0 g for Cu^{2+} and Pb^{2+}, respectively. The solution pH was maintained at 5.5, and initial metal concentrations of 150 and 400 mg L^{-1} for Cu^{2+} and Pb^{2+}, respectively, were used at corresponding contact times of 30 and 15 min.

A linear increase in the adsorption capacity and removal efficiency is observed for both heavy metal ions with increases in the adsorbent concentration to approximately 1.4 and 1.8 g for Cu^{2+} and Pb^{2+}, respectively (Fig. 5). The values are considered as the optimum doses of biochar for maximum respective metal adsorption. The Cu^{2+} adsorption capacity of banana biochar is again significantly lower than that of Pb^{2+} despite using more than double the initial Pb^{2+} concentration with half the contact time when compared to that of Cu^{2+}.

The trends observed for adsorption capacity and removal efficiency could be due to the greater surface area availability and higher number of active adsorption sites or the increased numbers of functional groups with increases in the biochar dose that result in stronger metal cation–biochar interactions [46,47]. When the adsorbent dose is increased above the optimum dose value that is determined for each metal ion, the adsorption capacity reduces due to unsaturation of adsorption sites since the dose of the biochar was increased at fixed concentrations of Cu^{2+} and Pb^{2+} [48].

3.2.4 Effects of the Initial Metal Concentrations

The effects of the initial metal concentrations on the adsorption capacity and removal efficiency of the biochar were examined by varying the Cu^{2+} and Pb^{2+} concentrations from 50 to 300 and 100 to 1000 mg L^{-1}, respectively (Fig. 6a, b). For the batch experiment, the pH of the solution was kept constant at 5.5 by using an adsorbent dose of 1.0 and 0.5 g with 30 and 15 min contact time for Cu^{2+} and Pb^{2+}, respectively.

The adsorption capacity increases by approximately 100 and 150 mg g^{-1} when the Cu^{2+} and Pb^{2+} concentrations increase from 50 to 300 mg L^{-1} and 100 to 1000 mg L^{-1}, respectively, as shown in Fig. 6a and b. Nevertheless, the metal removal efficiency of the biochar decreases by approximately 50% for Cu^{2+} (Fig. 6a) and by approximately 70% for Pb^{2+} (Fig. 6b) when the initial metal concentrations increase as described. The optimum Cu^{2+} and Pb^{2+} concentrations are observed as 200 and 700 mg L^{-1}, respectively, as shown in Fig. 6. A relatively high adsorption capacity of Pb^{2+} when compared with that of Cu^{2+} is achieved under batch conditions with half the adsorbent dose and contact time (0.5 g and 15 min, respectively) for Pb^{2+} when compared with those of Cu^{2+}. A decrease in removal efficiency at higher initial concentrations could be due to the rapidly filled binding sites and saturation of sorption sites on the surface of the adsorbent [49,50]. Additionally, the increase in the driving force of adsorption with an increase in the initial metal concentration

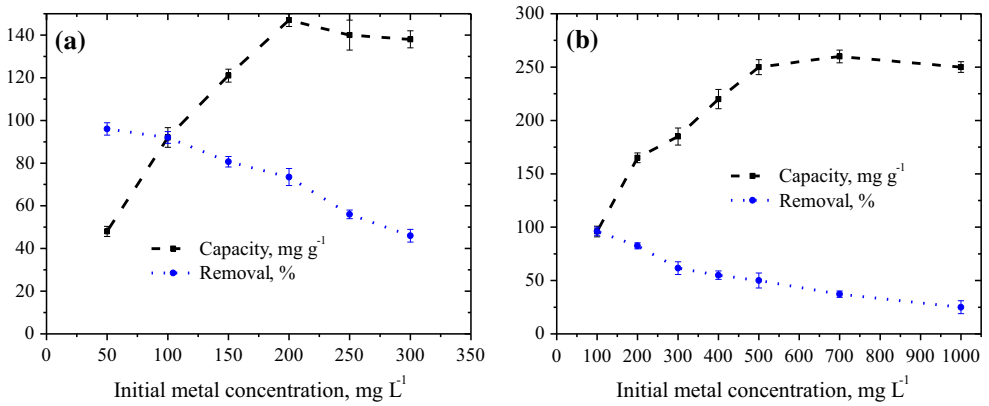

Fig. 6 Effects of initial metal concentration on the metal adsorption capacity of Cu^{2+} (**a**) and Pb^{2+} (**b**) (initial pH 5.5, contact time 30 and 15 min with adsorbent dose 1.0 and 0.5 g for Cu^{2+} and Pb^{2+}, respectively)

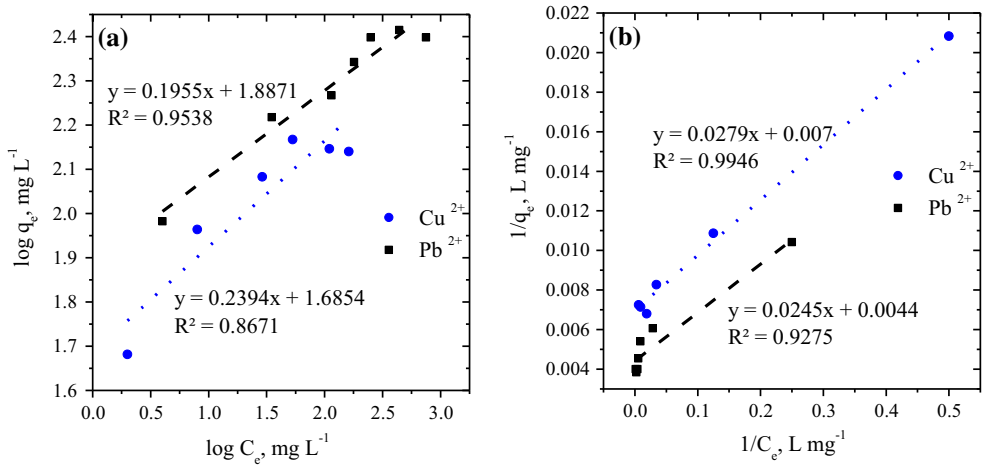

Fig. 7 Linearized Freundlich and Langmuir adsorption isotherms for Cu^{2+} and Pb^{2+} biosorption

leads to the saturation of the sorption sites on the surface of the adsorbent, and this results in decreased adsorption capacity [51,52].

3.3 Equilibrium Isotherm Models and Adsorption Kinetics

3.3.1 Isotherm Models

Different isotherm models including Langmuir, Freundlich, Temkin, Halsey, Harkin–Jura (H–R), and Dubinin–Radush kevich (D–R) were applied to correlate the adsorption capacity and residual adsorbate concentration. The experimental data for heavy metal ion adsorption were further analyzed by using different isotherm models to describe the adsorption of the solutes. The analyses were performed at 30 °C and at pH 5.5 for 150 and 400 mg L^{-1} initial Cu^{2+} and Pb^{2+} concentrations by using adsorbent doses of 0.5 and 1 g with contact times corresponding to 30 and 15 min, respectively.

The Freundlich isotherm model describes the adsorption of a heterogeneous system by assuming multilayer adsorption and is expressed in a linearized form as shown in Eq. (3) as follows:

$$\log q_e = \log K_F + \frac{1}{n}\log C_e \tag{3}$$

where q_e (mg g^{-1}) denotes the amount of metal ions adsorbed at equilibrium, C_e (mg L^{-1}) denotes the metal ion concentration in solution, K_F (L g^{-1}) denotes the relative adsorption capacity, and $1/n$ denotes the heterogeneity factor (adsorption intensity). The fit of the equilibrium data to the Freundlich isotherm is evaluated by using a plot of log q_e versus log C_e (Fig. 7a) while K_F and $1/n$ are, respectively, calculated from the intercept and slope of the linear plot (Table 1). The latter determines the intensity and feasibility of the adsorption process.

As observed in Table 1, the values of K_F and $1/n$ for Cu^{2+} are 56.82 and 0.239 mg g^{-1} ($n = 4.18$), respectively, and this indicates that the adsorption of Cu^{2+} is favorable as the value

Table 1 Parameters obtained from different isotherm models for the adsorption of Cu^{2+} and Pb^{2+} on the biochar

Isotherm	Parameter	Cu^{2+}	Pb^{2+}
Freundlich	$q_{e,exp}$. mg g^{-1}	147	260
	K_F, L g^{-1}	56.82	79.1
	N	4.18	5.12
	R^2	0.867	0.954
Langmuir	q_{max}, mg g^{-1}	142.86	227.27
	K_{ads}, L mg^{-1}	0.251	0.1796
	R^2	0.995	0.928
Temkin	A_T, L mg^{-1}	7.138	4.567
	b_T, kJ mol^{-1}	116.437	77.3087
	R^2	0.901	0.945
Halsey	$q_{e\,cal}$, mg g^{-1}	163.804	281.301
	n_H	−4.177	−5.115
	k_H	16.21	22.23
	R^2	0.867	0.954
Harkin–Jura	A, mg g^{-1}	5000	25000
	B	2	2.5
	R^2	0.736	0.87
Dubinin–Radushkevich	q_{DR}, mol g^{-1}	140.008	227.08
	β, $(mol\ kJ^{-1})^2$	0.0006	0.0008
	E, kJ mol^{-1}	16.08	12.25
	R^2	0.974	0.845

of n lies in the range of 2–10. The adsorption of Pb^{2+} is also favorable as its n value is 5.12, given in Table 1. Additionally, the slightly higher value (0.954) of the coefficient of determination (R^2) for Pb^{2+} that is obtained with the Freundlich isotherm when compared to that with the Langmuir isotherm (0.928) indicates that the equilibrium data for the adsorption of Pb^{2+} are in better agreement with the Freundlich isotherm model.

The linearized form of the Langmuir model that assumes monolayer coverage is expressed as Eq. (4) as follows:

$$\frac{1}{q_e} = \frac{1}{q_{max}} + \left(\frac{1}{q_{max} K_{ads}}\right)\frac{1}{C_e} \tag{4}$$

where q_{max} denotes the maximum metal concentration attained in the monolayer coverage, and K_{ads} (L mg^{-1}) denotes the Langmuir adsorption constant. The fit of the equilibrium data to the Langmuir isotherm is evaluated by using a plot of $1/q_e$ versus $1/C_e$ (Fig. 7b) and q_{max} and K_{ads} are calculated by using the intercept and slope values of the plot, respectively, given in Table 1.

The R^2 for the fit of Cu^{2+} adsorption data to the Langmuir isotherm is 0.995 (Table 1), and this reflects the suitability of this model for describing the adsorption of Cu^{2+} on the biochar. The predicted maximum adsorption capacity (q_{max}) is lower than the experimentally attained values, and this indicates the possibility of these adsorbents reaching their saturation capacity at lower initial metal concentrations (Table 1).

The Temkin isotherm model covers the adsorbate–adsorbent interaction [53] by assuming a uniform distribution of binding energies at the adsorbent surface [54] and is expressed in a linearized form as Eq. (5) as follows:

$$q_e = B_T \ln A_T + B_T \ln C_e \tag{5}$$

where A_T (L g^{-1}) denotes the equilibrium binding constant that indicates the maximum binding energy, b_T (B_TRT, kJ mol^{-1}) denotes a constant related to the heat of adsorption, T denotes the absolute temperature (K), and R denotes the universal gas constant (8.314 J mol^{-1} K^{-1}). A plot of q_e relative to ln C_e is used to determine the constants that are listed in Table 1.

The Temkin model does not usually perform well while predicting liquid-phase adsorption isotherms (complex adsorption systems) [55]. This is also reflected in the study based on the value of R^2 (0.901 for Cu^{2+}, Table 1), which indicates that the model exhibits a poorer fit to the equilibrium data when compared to the Langmuir and Freundlich isotherm models.

A good fit of the Halsey isotherm confirms the heterogeneous nature of the adsorbent and is typically suitable for multilayer adsorption. The linearized form of the Halsey isotherm is expressed using Eq. (6) as follows:

$$\ln q_e = \frac{1}{n_H} k_H - \frac{1}{n_H} \ln C_e \tag{6}$$

where k_H and n_H denote Halsey's isotherm constants and are calculated from the slope and intercept of the plot of ln q_e relative to ln C_e, respectively.

Table 1 presents the relatively better agreement that is obtained with a fit of the Halsey isotherm to the adsorption data of Pb^{2+} ($R^2 = 0.954$) when compared to either the Langmuir or the Temkin isotherms. This confirms the heterogeneous nature of the biochar. Furthermore, the calculated value of q_e slightly exceeds the experimental values that are determined for both Cu^{2+} and Pb^{2+} (163 mg g^{-1} when compared with 147 mg g^{-1} for Cu^{2+}, and 281 mg g^{-1} when compared with 263 mg g^{-1} for Pb^{2+}), given in Table 1, and this also confirms the good representation of the equilibrium data using the model.

The linearized form of the H–J isotherm model assumes multilayer adsorption on the surface of the adsorbent with heterogeneous pore distribution [56] is expressed using Eq. (7) as follows:

$$\frac{1}{q_e^2} = B/A - \left(\frac{1}{A}\right)\log C_e \tag{7}$$

Table 2 Pseudo-second-order adsorption rate constants and calculated q_e at different initial concentrations of Cu^{2+} and Pb^{2+} on banana biochar at 30 °C and pH = 5.5

	$q_{e\,exp}$ (mg g^{-1})	$q_{e\,cal}$ (mg g^{-1})	k_2 (g mg^{-1} min^{-1})	h (mg g^{-1} min^{-1})	R^2
Initial Cu^{2+} conc. (mg L^{-1})					
100	92	99	0.011	78.696	1
150	121	123.457	0.0075	114.943	0.99
200	147	147.059	0.0052	112.36	0.99
300	138	149.25	0.0048	106.383	0.99
Initial Pb^{2+} conc. (mg L^{-1})					
200	165	175.439	0.0026	81.301	0.99
400	220	222.2229	0.0023	114.943	0.99
600	270	256.419	0.0127	130	0.99
800	280	285.7149	0.0016	133.333	1

where B and A denote H–J constants obtained from the slope and intercept values, respectively, of a plot of $1/q_e^2$ relative to log C_e, given in Table 1. A poor fit to the adsorption data was obtained for both Cu^{2+} and Pb^{2+} as reflected in the R^2 values (0.736 and 0.87 for Cu^{2+} and Pb^{2+}, respectively). The D–R isotherm (Eq. 8) is generally applied to distinguish between the physical and chemical adsorptions of metal ions with its mean free energy and often provides a good fit for data at high solute activities and at an intermediate range of concentrations [57,58] as follows:

$$\ln q_e = \ln q_{DR} - \beta\,\varepsilon^2 \tag{8}$$

where q_{DR} denotes the theoretical isotherm saturation capacity (mg g^{-1}), β denotes the constant of the adsorption energy (mol^2 kJ^{-2}), and ε denotes the Polanyi potential (RT ln(1+1/C_e)). Values of q_{DR} and β are calculated from the intercept and slope, respectively, of the plot of ln q_e relative to RT ln(1+1/C_e). The values are presented in Table 1. A high value of R^2 (0.974, Table 1) when compared with those of other isotherm models with the exception of the Langmuir model indicates the suitability of the model for Cu^{2+} adsorption. However, a low value of R^2 for Pb^{2+} (0.845, Table 1) reflects a poor fit to the experimental equilibrium data when compared to other models.

In order to distinguish between physical and chemical adsorption, the mean free energy of adsorption ($E = \frac{1}{\sqrt{2\beta}}$) is computed in the D-R isotherm model to assess as to whether the adsorption process is physical ($E < 8$ kJ mol^{-1}) or chemical ($E = 8 - 16$ kJ mol^{-1}). As shown in Table 1, the E values for Cu^{2+} and Pb^{2+} are 15.08 and 12.25 kJ mol^{-1}, respectively, and they reflect the chemisorption of both the studied metal ions on the biochar.

3.3.2 Adsorption Kinetics

Various initial concentrations of Cu^{2+} (100, 150, 200, and 300 mg L^{-1}) and Pb^{2+} (200, 400, 600, and 800 mg L^{-1}) were selected to determine the rate of adsorption as listed in Table 2. Both pseudo-first-order and pseudo-second-order kinetic models were applied over variable time increments of 5–10 min up to 1 h and at 1 h time increments from 1 to 6 h of adsorption. A solution temperature of 30 °C and a pH value of 5.5 were used with an adsorbent dose of biochar of 1 and 0.5 g for Cu^{2+} and Pb^{2+}, respectively. The linearized form of the pseudo-first-order and pseudo-second-order kinetic models are expressed by using Eqs. (9) and (10), respectively, as follows:

$$\log(q_e - q_t) = \log q_e - \frac{k_1}{2.303}t \tag{9}$$

$$\frac{t}{q_t} = \frac{1}{k_2 q_e^2} + \frac{1}{q_e}t \tag{10}$$

where q_e denotes the amount of metal ions adsorbed at equilibrium per unit mass of adsorbent (mg g^{-1}) and q_t denotes the amount of metal adsorbed at time t (mg g^{-1}). The pseudo-first-order rate constant, k_1 (h^{-1}), is determined from the slope of the plot of log ($q_e - q_t$) relative to t while the slope and intercept values of the plot of t/q_t relative to t is used to determine the pseudo-second-order rate constant, k_2 (g mg^{-1} min^{-1}). A poor correlation with the experimental data is observed by using an initial concentration of 200 mg L^{-1} for both Cu^{2+} and Pb^{2+} in the pseudo-first-order kinetic model as expressed by the R^2 values (0.3–0.45) shown in Fig. 8a and b.

Nevertheless, extremely high R^2 values (close to unity) were observed for the pseudo-second-order model for both Cu^{2+} and Pb^{2+} while using the same initial metal concentration of 200 mg L^{-1} (Fig. 8a, b). Similarly, a linear relationship was displayed for other initial metal concentrations of Cu^{2+} and Pb^{2+} in the pseudo-second-order kinetic model as expressed by the R^2 values shown in Table 2.

The calculated values of q_e agreed well with the experimental adsorption capacities ($q_{e\,exp}$) at different initial metal concentrations of Cu^{2+} and Pb^{2+} as listed in Table 2, and this indicated that the pseudo-second-order model is more

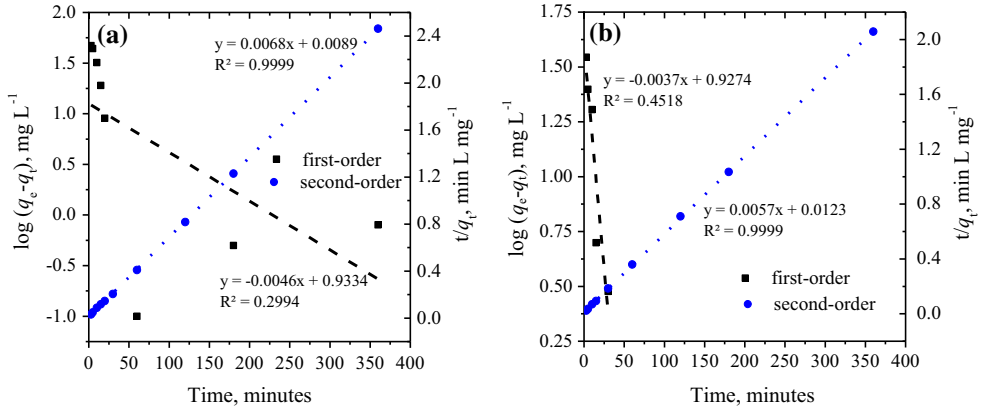

Fig. 8 Pseudo-first-order and second-order kinetic plots with 200 mg L^{-1} initial solution concentration of Cu^{2+} (**a**), and Pb^{2+} (**b**)

likely to describe the kinetic behavior of metal adsorption on the banana biochar when compared to the other models. The initial adsorption rate, $h = k_2 q_e^2$ (mg g^{-1} min^{-1}), is also calculated for each initial concentration condition and shown in Table 2. The pseudo-second-order kinetic model is based on solid-phase sorption of divalent metals [59,60], and the good fit of this model supports the assumption that chemisorption corresponds to the rate-controlling step for the adsorption of Cu^{2+} and Pb^{2+} on the banana biochar.

4 Conclusions

In this study, the use of biochar from banana peel for adsorption of Cu^{2+} and Pb^{2+} was investigated and batch experiments were performed in triplicate to optimize a range of process parameters. The adsorbent was characterized by using SEM, XRD, FTIR, and BET. Two-parameter isotherm models were used to analyze the behavior of the adsorption process, and pseudo-first-order and pseudo-second-order kinetics were applied to the adsorption kinetics data.

The results did not indicate any significant changes in the adsorption capacity after approximately 30 min, and the equilibrium time was reached at approximately 90 min. The removal efficiency of Cu^{2+} was significantly lower than that of Pb^{2+} at the same adsorbent dose and/or initial metal concentration. The adsorption capacity and the removal efficiency of both heavy metal ions increased by approximately 40–50% when the solution pH increased from 3 to 9, and the optimum pH values were determined as 5.5 and 9 for Cu^{2+} and Pb^{2+}, respectively. Given the higher surface area and availability of additional adsorption sites, an increase in the dose of the biochar from 0.2 to 2.5 g caused a linear increase in metal adsorption, and an adsorbent dose of approximately 1.5 g was considered the optimum dose. Finally, decreases of 50 and 70% in the removal efficiency of Cu^{2+} and Pb^{2+}, respectively, were observed when the initial metal concentrations were increased from 50 to 300 mg L^{-1} for Cu^{2+} and from 200 to 1000 mg L^{-1} for Pb^{2+}.

The Langmuir model agreed well with the experimental data for the adsorption of Cu^{2+} based on the R^2 value. With respect to the other isotherms, the experimental adsorption data exhibited the best fit with models in the following order: D–R> Temkin > Freundlich and Halsey > H–J. The adsorption data of Pb^{2+} exhibited the best fit with models in the following order: Freundlich and Halsey > Temkin > Langmuir > H–J > D–R. The results indicated a poor correlation with the pseudo-first-order kinetic model while the pseudo-second-order kinetic model better described the adsorption behavior and provided R^2 values close to 1.0 for both Cu^{2+} and Pb^{2+}. This suggested the chemisorption property of the banana biochar. The results demonstrated the effective absorption potential of the banana biochar for Cu^{2+} and Pb^{2+} and indicated that the use of this low-cost agricultural waste for applications in wastewater treatment is encouraging given suitable pre-treatment and modifications to enhance its performance.

Acknowledgements The project was financially supported by King Saud University, Vice Deanship of Research Chairs.

Compliance with Ethical Standards

Conflict of interest Authors declare no conflict of interest.

References

1. Ajmal, M.; Ali Khan Rao, R.; Anwar, S.; Ahmad, J.; Ahmad, R.: Adsorption studies on rice husk: removal and recovery of Cd(II) from wastewater. Bioresour. Technol. **86**, 147–149 (2003). https://doi.org/10.1016/S0960-8524(02)00159-1
2. Mahugo-Santana, C.; Sosa-Ferrera, Z.; Torres-Padrón, M.E.; Santana-Rodríguez, J.J.: Application of new approaches to liquid-phase microextraction for the determination of emerging pollutants. TrAC, Trends Anal. Chem. **30**, 731–748 (2011). https://doi.org/10.1016/j.trac.2011.01.011

3. Amuda, O.S.; Giwa, A.A.; Bello, I.A.: Removal of heavy metal from industrial wastewater using modified activated coconut shell carbon. Biochem. Eng. J. **36**, 174–181 (2007). https://doi.org/10.1016/j.bej.2007.02.013
4. Singh, R.; Gautam, N.; Mishra, A.; Gupta, R.: Heavy metals and living systems: An overview. Indian J. Pharmacol. **43**, 246–253 (2011). https://doi.org/10.4103/0253-7613.81505
5. Amin, M.T.; Alazba, A.A.; Shafiq, M.: Adsorption of copper (Cu^{2+}) from aqueous solution using date palm trunk fibre: isotherms and kinetics. Desalination Water Treat. **57**, 22454–22466 (2016). https://doi.org/10.1080/19443994.2015.1131635
6. Jarup, L.: Hazards of heavy metal contamination. Br. Med. Bull. **68**, 167–182 (2003). https://doi.org/10.1093/bmb/ldg032
7. Sridhara Chary, N.; Kamala, C.T.; Samuel Suman Raj, D.: Assessing risk of heavy metals from consuming food grown on sewage irrigated soils and food chain transfer. Ecotoxicol. Environ. Saf. **69**, 513–524 (2008). https://doi.org/10.1016/j.ecoenv.2007.04.013
8. Tchounwou, P.B.; Yedjou, C.G.; Patlolla, A.K.; Sutton, D.J.: Heavy Metals Toxicity and the Environment. EXS. **101**, 133–164 (2012). https://doi.org/10.1007/978-3-7643-8340-4_6
9. Jaishankar, M.; Tseten, T.; Anbalagan, N.; Mathew, B.B.; Beeregowda, K.N.: Toxicity, mechanism and health effects of some heavy metals. Interdiscip. Toxicol. **7**, 60–72 (2014). https://doi.org/10.2478/intox-2014-0009
10. Kumar, M.; Gogoi, A.; Kumari, D.; Borah, R.; Das, P.; Mazumder, P.; Tyagi, V.K.: Review of perspective, problems, challenges, and future scenario of metal contamination in the urban environment. J. Hazard. Toxic Radioact. Waste **21**, 04017007 (2017)
11. Hegazi, H.A.: Removal of heavy metals from wastewater using agricultural and industrial wastes as adsorbents. HBRC J. **9**, 276–282 (2013). https://doi.org/10.1016/j.hbrcj.2013.08.004
12. Wan Ngah, W.S.; Hanafiah, M.A.K.M.: Removal of heavy metal ions from wastewater by chemically modified plant wastes as adsorbents: A review. Bioresour. Technol. **99**, 3935–3948 (2008). https://doi.org/10.1016/j.biortech.2007.06.011
13. Ahmad, T.; Danish, M.; Rafatullah, M.; Ghazali, A.; Sulaiman, O.; Hashim, R.; Ibrahim, M.N.M.: The use of date palm as a potential adsorbent for wastewater treatment: a review. Environ. Sci. Pollut. Res. **19**, 1464–1484 (2011). https://doi.org/10.1007/s11356-011-0709-8
14. Ahmaruzzaman, M.; Gupta, V.K.: Rice husk and its ash as low-cost adsorbents in water and wastewater treatment. Ind. Eng. Chem. Res. **50**, 13589–13613 (2011). https://doi.org/10.1021/ie201477c
15. Guo, Y.; Zhu, W.; Li, G.; Wang, X.; Zhu, L.: Effect of alkali treatment of wheat straw on adsorption of Cu(II) under acidic condition. J. Chem. **2016**, e6326372 (2016). https://doi.org/10.1155/2016/6326372
16. Li, W.; Zhang, L.; Peng, J.; Li, N.; Zhang, S.; Guo, S.: Tobacco stems as a low cost adsorbent for the removal of Pb(II) from wastewater: equilibrium and kinetic studies. Ind. Crops Prod. **28**, 294–302 (2008). https://doi.org/10.1016/j.indcrop.2008.03.007
17. Rajput, M.S.; Sharma, A.; Sharma, S.; Verma, S.: Removal of lead (II) from aqueous solutions by orange peel. Int. J. Appl. Res. **1**, 411–413 (2015)
18. Patra, J.M.; Panda, S.S.; Dhal, N.K.: Biochar as a low-cost adsorbent for heavy metal removal: a review. Int. J. Res. Biosci. **6**, 1–7 (2017)
19. Tang, J.; Zhu, W.; Kookana, R.; Katayama, A.: Characteristics of biochar and its application in remediation of contaminated soil. J. Biosci. Bioeng. **116**, 653–659 (2013). https://doi.org/10.1016/j.jbiosc.2013.05.035
20. Inyang, M.; Gao, B.; Yao, Y.; Xue, Y.; Zimmerman, A.R.; Pullammanappallil, P.; Cao, X.: Removal of heavy metals from aqueous solution by biochars derived from anaerobically digested biomass. Bioresour. Technol. **110**, 50–56 (2012). https://doi.org/10.1016/j.biortech.2012.01.072
21. Inyang, M.I.; Gao, B.; Yao, Y.; Xue, Y.; Zimmerman, A.; Mosa, A.; Pullammanappallil, P.; Ok, Y.S.; Cao, X.: A review of biochar as a low-cost adsorbent for aqueous heavy metal removal. Crit. Rev. Environ. Sci. Technol. **46**, 406–433 (2016). https://doi.org/10.1080/10643389.2015.1096880
22. Liu, H.Q.; Xu, X.; Wu, Z.H.; Wei, G.X.; Sun, L.: Removal of heavy metals from aqueous solution using biochar derived from biomass and sewage sludge. Appl. Mech. Mater. **768**, 89–95 (2015). https://doi.org/10.4028/www.scientific.net/AMM.768.89
23. Mary, G.S.; Sugumaran, P.; Niveditha, S.; Ramalakshmi, B.; Ravichandran, P.; Seshadri, S.: Production, characterization and evaluation of biochar from pod (Pisum sativum), leaf (Brassica oleracea) and peel (Citrus sinensis) wastes. Int. J. Recycl. Org. Waste Agric. **5**, 43–53 (2016). https://doi.org/10.1007/s40093-016-0116-8
24. Mohan, D.; Sarswat, A.; Ok, Y.S.; Pittman, C.U.: Organic and inorganic contaminants removal from water with biochar, a renewable, low cost and sustainable adsorbent-a critical review. Bioresour. Technol. **160**, 191–202 (2014). https://doi.org/10.1016/j.biortech.2014.01.120
25. Niazi, N.K.; Murtaza, B.; Bibi, I.; Shahid, M.; White, J.C.; Nawaz, M.F.; Bashir, S.; Shakoor, M.B.; Choppala, G.; Murtaza, G.; Wang, H.: Chapter 7: removal and recovery of metals by biosorbents and biochars derived from Biowastes. In: Environmental Materials and Waste. pp. 149–177. Academic Press (2016)
26. Rajapaksha, A.U.; Chen, S.S.; Tsang, D.C.W.; Zhang, M.; Vithanage, M.; Mandal, S.; Gao, B.; Bolan, N.S.; Ok, Y.S.: Engineered/designer biochar for contaminant removal/immobilization from soil and water: potential and implication of biochar modification. Chemosphere **148**, 276–291 (2016). https://doi.org/10.1016/j.chemosphere.2016.01.043
27. Tan, X.; Liu, Y.; Zeng, G.; Wang, X.; Hu, X.; Gu, Y.; Yang, Z.: Application of biochar for the removal of pollutants from aqueous solutions. Chemosphere **125**, 70–85 (2015). https://doi.org/10.1016/j.chemosphere.2014.12.058
28. Ahmad, M.; Rajapaksha, A.U.; Lim, J.E.; Zhang, M.; Bolan, N.; Mohan, D.; Vithanage, M.; Lee, S.S.; Ok, Y.S.: Biochar as a sorbent for contaminant management in soil and water: a review. Chemosphere **99**, 19–33 (2014). https://doi.org/10.1016/j.chemosphere.2013.10.071
29. DeMessie, B.; Sahle-Demessie, E.; Sorial, G.A.: Cleaning water contaminated with heavy metal ions using pyrolyzed biochar adsorbents. Sep. Sci. Technol. **50**, 2448–2457 (2015). https://doi.org/10.1080/01496395.2015.1064134
30. Tag, A.T.; Duman, G.; Ucar, S.; Yanik, J.: Effects of feedstock type and pyrolysis temperature on potential applications of biochar. J. Anal. Appl. Pyrolysis. **120**, 200–206 (2016). https://doi.org/10.1016/j.jaap.2016.05.006
31. Karim, A.; Kumar, M.; Mohapatra, S.; Panda, C.; Singh, A.: Banana peduncle biochar: characteristics and adsorption of hexavalent chromium from aqueous solution. Int. Res. J. Pure Appl. Chem. **7**, 1–10 (2015). https://doi.org/10.9734/IRJPAC/2015/16163
32. Minello, M.C.S.; Paçó, A.L.; Martines, M.A.U.; Caetano, L.; Santos, A.D.; Padilha, P.M.; Castro, G.R.: Sediment grain size distribution and heavy metals determination in a dam on the Paraná River at Ilha Solteira, Brazil. J. Environ. Sci. Health. A **44**, 861–865 (2009). https://doi.org/10.1080/10934520902958591
33. Aslam, M.M.; Hasan, I.; Malik, M.; Matin, A.: Removal of copper from industrial effluent by adsorption with economically viable material. Electron. J. Environ. Agric. Food Chem. **3**, 658–664 (2004)
34. László, K.; Bóta, A.; Nagy, L.G.: Comparative adsorption study on carbons from polymer precursors. Carbon **38**, 1965–1976 (2000). https://doi.org/10.1016/S0008-6223(00)00038-5
35. Yang, G.; Wang, Z.; Xian, Q.; Shen, F.; Sun, C.; Zhang, Y.; Wu, J.: Effects of pyrolysis temperature on the physicochemical proper-

ties of biochar derived from vermicompost and its potential use as an environmental amendment. RSC Adv. **5**, 40117–40125 (2015). https://doi.org/10.1039/C5RA02836A
36. Ho, Y.S.; Ng, J.C.Y.; McKay, G.: Kinetics of pollutant sorption by biosorbents: review. Sep. Purif. Methods **29**, 189–232 (2000). https://doi.org/10.1081/SPM-100100009
37. Krishnan, K.A.; Anirudhan, T.S.: Removal of cadmium(II) from aqueous solutions by steam-activated sulphurised carbon prepared from sugar-cane bagasse pith: kinetics and equilibrium studies. Water SA. **29**, 147–156 (2003). https://doi.org/10.4314/wsa.v29i2.4849
38. Qadeer, R.; Akhtar, S.: Kinetics study of lead ion adsorption on active carbon. Turk. J. Chem. **29**, 95–100 (2005)
39. Areco, M.M.; dos Afonso, M.S.: Copper, zinc, cadmium and lead biosorption by *Gymnogongrus torulosus*. Thermodynamics and kinetics studies. Colloids Surf. B Biointerfaces. **81**, 620–628 (2010). https://doi.org/10.1016/j.colsurfb.2010.08.014
40. O'Connell, D.W.; Birkinshaw, C.; O'Dwyer, T.F.: Heavy metal adsorbents prepared from the modification of cellulose: a review. Bioresour. Technol. **99**, 6709–6724 (2008). https://doi.org/10.1016/j.biortech.2008.01.036
41. Al-Ghouti, M.A.; Li, J.; Salamh, Y.; Al-Laqtah, N.; Walker, G.; Ahmad, M.N.M.: Adsorption mechanisms of removing heavy metals and dyes from aqueous solution using date pits solid adsorbent. J. Hazard. Mater. **176**, 510–520 (2010). https://doi.org/10.1016/j.jhazmat.2009.11.059
42. Al-Ghouti, M.A.; Khraisheh, M.A.M.; Allen, S.J.; Ahmad, M.N.: The removal of dyes from textile wastewater: a study of the physical characteristics and adsorption mechanisms of diatomaceous earth. J. Environ. Manage. **69**, 229–238 (2003). https://doi.org/10.1016/j.jenvman.2003.09.005
43. Chen, J.P.; Lin, M.: Equilibrium and kinetics of metal ion adsorption onto a commercial H-type granular activated carbon: experimental and modeling studies. Water Res. **35**, 2385–2394 (2001). https://doi.org/10.1016/S0043-1354(00)00521-2
44. Pehlivan, E.; Yanık, B.H.; Ahmetli, G.; Pehlivan, M.: Equilibrium isotherm studies for the uptake of cadmium and lead ions onto sugar beet pulp. Bioresour. Technol. **99**, 3520–3527 (2008). https://doi.org/10.1016/j.biortech.2007.07.052
45. Dronnet, V.M.; Renard, C.M.G.C.; Axelos, M.A.V.; Thibault, J.-F.: Binding of divalent metal cations by sugar-beet pulp. Carbohydr. Polym. **34**, 73–82 (1997). https://doi.org/10.1016/S0144-8617(97)00055-6
46. Ofomaja, A.E.; Ho, Y.-S.: Equilibrium sorption of anionic dye from aqueous solution by palm kernel fibre as sorbent. Dyes Pigm. **74**, 60–66 (2007). https://doi.org/10.1016/j.dyepig.2006.01.014
47. Uzunoğlu, D.; Gürel, N.; Özkaya, N.; Özer, A.: The single batch biosorption of copper(II) ions on Sargassum acinarum. Desalination Water Treat. **52**, 1514–1523 (2014). https://doi.org/10.1080/19443994.2013.789403
48. Huang, X.-Y.; Mao, X.-Y.; Bu, H.-T.; Yu, X.-Y.; Jiang, G.-B.; Zeng, M.-H.: Chemical modification of chitosan by tetraethylenepentamine and adsorption study for anionic dye removal. Carbohydr. Res. **346**, 1232–1240 (2011). https://doi.org/10.1016/j.carres.2011.04.012
49. Al-Homaidan, A.A.; Al-Houri, H.J.; Al-Hazzani, A.A.; Elgaaly, G.; Moubayed, N.M.S.: Biosorption of copper ions from aqueous solutions by Spirulina platensis biomass. Arab. J. Chem. **7**, 57–62 (2014). https://doi.org/10.1016/j.arabjc.2013.05.022
50. Putra, W.P.; Kamari, A.; Yusoff, S.N.M.; Ishak, C.F.; Mohamed, A.; Hashim, N.; Isa, I.M.: Biosorption of Cu(II), Pb(II) and Zn(II) Ions from aqueous solutions using selected waste materials: adsorption and characterisation studies. J. Encapsulation Adsorpt. Sci. **04**, 25 (2014). https://doi.org/10.4236/jeas.2014.41004
51. Bhaumik, M.; Setshedi, K.; Maity, A.; Onyango, M.S.: Chromium(VI) removal from water using fixed bed column of polypyrrole/Fe3O4 nanocomposite. Sep. Purif. Technol. **110**, 11–19 (2013). https://doi.org/10.1016/j.seppur.2013.02.037
52. Malkoc, E.; Nuhoglu, Y.; Dundar, M.: Adsorption of chromium(VI) on pomace–an olive oil industry waste: batch and column studies. J. Hazard. Mater. **138**, 142–151 (2006). https://doi.org/10.1016/j.jhazmat.2006.05.051
53. Temkin, M.J.; Pyzhev, V.: Kinetics of ammonia synthesis on promoted iron catalysts. Acta Physicochim URSS. **12**, 217–222 (1940)
54. Kumar, P.S.; Ramakrishnan, K.; Gayathri, R.: Removal of Nickel(II) from aqueous solutions by ceralite IR 120 cationic exchange resins. J. Eng. Sci. Technol. **5**, 232–243 (2010)
55. Tahir, H.; Hammed, U.; Sultan, M.; Jahanzeb, Q.: Batch adsorption technique for the removal of malachite green and fast green dyes by using montmorillonite clay as adsorbent. Afr. J. Biotechnol. **9**, 8206–8214 (2010). https://doi.org/10.5897/AJB10.911
56. Almeida, C.A.P.; Debacher, N.A.; Downs, A.J.; Cottet, L.; Mello, C.A.D.: Removal of methylene blue from colored effluents by adsorption on montmorillonite clay. J. Colloid Interface Sci. **332**, 46–53 (2009). https://doi.org/10.1016/j.jcis.2008.12.012
57. Dąbrowski, A.: Adsorption—from theory to practice. Adv. Colloid Interface Sci. **93**, 135–224 (2001). https://doi.org/10.1016/S0001-8686(00)00082-8
58. Günay, A.; Arslankaya, E.; Tosun, İ.: Lead removal from aqueous solution by natural and pretreated clinoptilolite: adsorption equilibrium and kinetics. J. Hazard. Mater. **146**, 362–371 (2007). https://doi.org/10.1016/j.jhazmat.2006.12.034
59. Yadav, S.K.; Singh, D.K.; Sinha, S.: Adsorption study of lead(II) onto xanthated date palm trunk: kinetics, isotherm and mechanism. Desalination Water Treat. **51**, 6798–6807 (2013). https://doi.org/10.1080/19443994.2013.792142
60. Liang, S.; Guo, X.; Feng, N.; Tian, Q.: Effective removal of heavy metals from aqueous solutions by orange peel xanthate. Trans. Nonferrous Met. Soc. China **20**, s187–s191 (2010). https://doi.org/10.1016/S1003-6326(10)60037-4